

Properties of anisotropic magnetic impurities on surfaces

R. Žitko,^{1,2} R. Peters,¹ and Th. Pruschke¹

¹*Institute for Theoretical Physics, University of Göttingen,
Friedrich-Hund-Platz 1, D-37077 Göttingen, Germany*

²*J. Stefan Institute, Jamova 39, SI-1000 Ljubljana, Slovenia*

(Dated: March 22, 2022)

Using numerical renormalization group techniques, we study static and dynamic properties of a family of single-channel Kondo impurity models with axial magnetic anisotropy DS_z^2 terms; such models are appropriate to describe magnetic impurity atoms adsorbed on non-magnetic surfaces, which may exhibit surface Kondo effect. We show that for positive anisotropy D and for any spin S , the systems behave at low temperatures as regular Fermi liquids with fully compensated impurity spin. The approach to the stable fixed point depends on the value of the spin S and on the ratio $D/T_K^{(0)}$, where $T_K^{(0)}$ is the Kondo temperature in the absence of the anisotropy. For $S = 1$, the screening occurs in two stages if $D < T_K^{(0)}$; the second Kondo temperature is exponentially reduced in this case. More generally, there is an effective spin-1/2 Kondo effect for any integer S if $D < T_K^{(0)}$ and for any half-integer S if $D > T_K^{(0)}$. For negative anisotropy D , the system is a non-Fermi liquid with residual anisotropic exchange interaction. However, the presence of transverse magnetic anisotropy $E(S_x^2 - S_y^2)$ restores Fermi-liquid behavior in real systems.

PACS numbers: 75.30.Gw, 72.10.Fk, 72.15.Qm, 68.37.Ef

I. INTRODUCTION

As the sizes of the active components in magnetic devices shrink, the ratio of the surface area over bulk volume steadily increases and the importance of surface and interface effects grows. In the past, the focus has mostly been on the magnetic properties of clean surfaces, thin films, and interfaces in multilayers^{1,2,3,4}, but now magnetism of nanostructures is emerging as a new subfield with the aim of exploring and modifying the exchange interaction at the nanometer level. Given that the symmetry in the surface area is always reduced as compared to the bulk, more attention needs to be given to possible additional surface-induced magnetic anisotropy effects^{1,2,5,6,7,8,9,10,11}. Recently, magnetic anisotropy on surfaces studied at the atomic level has become a new focus of interest with potential applications in ultra-dense magnetic data storage. Using scanning tunneling spectroscopy, the magnetic anisotropy can be measured on the single-atom level by analyzing the splittings of magnetic excitation peaks as a function of the applied magnetic field^{8,10}. Magnetic anisotropy constants were found to be very large, often in the meV/atom range^{5,10,12}.

Single magnetic impurity atoms adsorbed on surfaces or buried in the near-surface regions can be described using quantum impurity models^{13,14} with anisotropy terms^{10,15}. The dominant anisotropy terms are of the form $\bar{D}(\mathbf{S} \cdot \mathbf{n})^2$, where \mathbf{n} is a vector along a privileged axis that is commonly chosen to be the z -axis^{15,16}. The most important contributions seem to arise from the local spin-orbit coupling, as the reduced symmetry leads to unequal hybridization of the different d -orbitals of the impurity atom^{17,18}. For an impurity buried in the near-surface region, D depends on the distance from the surface and oscillates in sign¹⁸.

Numerical calculations and experiments show that the magnetic anisotropy strongly depends on the microscopic details. Depending on the impurity species and on the substrate, dif-

ferent directions of the privileged axis may be found. Density functional theory calculation predict, for example, that perpendicular anisotropy is common for single adatoms on metallic surfaces¹⁹.

Spin-excitation spectroscopy using a scanning tunneling microscope (STM) has revealed a rich variety of different classes of behavior. For example, for Fe (spin-2) adatom on a thin CuN decoupling layer on a Cu surface, the anisotropy is negative with the z -axis in the surface plane, along the direction of nitrogen atoms, while for Mn (spin-5/2) on the same surface, the anisotropy is weaker but with an out-of-plane z -axis, however D is still negative¹⁰. No anomalies at the Fermi level (surface Kondo effect^{20,21,22,23,24}) are observed for $D < 0$ ¹⁰. For Co (spin-3/2) on CuN layer, the anisotropy D is positive and signatures of the Kondo effect are observed in tunneling spectra²⁵. These results strongly motivate a study of the entire family of the Kondo impurity models for various values of spin and for different signs and magnitudes of the magnetic anisotropy. Due to the low symmetry at the surface, it appears sufficient as a first approximation to consider coupling to a single conduction channel (the one with the largest exchange coupling constant); it is unlikely that coupling constants to two orthogonal channels would be equal under these conditions.

Similar impurity models with large anisotropies also appear in the context of single molecular magnets, e.g. Mn_{12} or Fe_8 . It was possible to attach metallic contacts to these molecules allowing for electron transport measurements^{26,27}. The molecules exhibit very large spin values ($S = 10$ for Mn_{12}) and a negative- D axial anisotropy term DS_z^2 , so that ground states with two polarized large-spin states are favored in the absence of quantum spin tunneling due to the transverse anisotropy $E(S_x^2 - S_y^2)$ terms^{28,29,30,31}.

Since the ultimate miniaturization limit appears to be storing information in the spin states of single magnetic atoms, it is important to study decoherence by possible magnetic

screening effects through nearby conduction electrons (Kondo effect), since the goal is to have long-lived large-spin magnetic impurity states. The appropriate model is thus the impurity Kondo model with additional anisotropy terms that we introduce in Sec. II. In Sec. III we relate these models by means of scaling equations to the Kondo models with XXZ anisotropic exchange coupling to the conduction band. Numerical renormalization group results are presented in Sec. IV where we compare calculations for $S = 1$, $S = 3/2$ and $S = 2$. $S = 3/2$ is a typical representative for all half-integer-spin models, $S = 2$ a typical representative for all integer-spin models, while $S = 1$ is a special case with some additional features when compared to higher integer spins. We present results both for static properties (magnetic susceptibility, impurity entropy) and for dynamic properties (spectral functions, dynamic magnetic susceptibility). This section also contains a discussion of the various fixed points, focusing on the non-Fermi-liquid behavior in the $D < 0$ models.

II. MODEL

A general approach to study the anisotropy effects of adsorbed impurity atoms would start with a multi-orbital Anderson model for the d -orbitals with a suitable hybridization function for the coupling with the substrate and with electron-electron repulsion and Hund coupling parameters extracted, for example, from density functional theory calculations. The next step would then consist of obtaining an effective Kondo-like model using a Schrieffer-Wolff transformation. We aim, however, to explore only the effects due to local magnetic anisotropy effects. We thus study a very simplified Kondo impurity model defined by the following Hamiltonian:

$$\begin{aligned} H &= H_{\text{band}} + H_{\text{K}} + H_{\text{aniso}}, \\ H_{\text{band}} &= \sum_{\mathbf{k}\sigma} \epsilon_{\mathbf{k}} c_{\mathbf{k}\sigma}^\dagger c_{\mathbf{k}\sigma}, \\ H_{\text{K}} &= J \mathbf{s} \cdot \mathbf{S}. \end{aligned} \quad (1)$$

Here operators $c_{\mathbf{k}\sigma}$ describe the conduction band electrons with momentum \mathbf{k} and spin $\sigma \in \{\uparrow, \downarrow\}$. In numerical calculations, we will for simplicity assume a flat band $\epsilon_{\mathbf{k}} = Wk$, where the dimensionless momentum (energy) k ranges from -1 to 1 and W is the half-bandwidth; the density of states is thus constant, $\rho = 1/(2W)$. Furthermore, the effective exchange constant J is defined as

$$J = \frac{1}{N^2} \sum_{\mathbf{k}\mathbf{k}'} J_{\mathbf{k},\mathbf{k}'}, \quad (2)$$

where $J_{\mathbf{k},\mathbf{k}'}$ describe exchange scattering of the conduction band electrons on the impurity, and the spin-density of the conduction band electrons \mathbf{s} is defined as

$$\mathbf{s} = \frac{1}{N} \sum_{\mathbf{k}\mathbf{k}'\alpha\alpha'} \frac{J_{\mathbf{k},\mathbf{k}'}}{J} c_{\mathbf{k}\alpha}^\dagger \left(\frac{1}{2} \boldsymbol{\sigma}_{\alpha\alpha'} \right) c_{\mathbf{k}'\alpha'}. \quad (3)$$

If $J_{\mathbf{k},\mathbf{k}'} \equiv J$ is constant, then \mathbf{s} can be interpreted as the spin-density of conduction band electrons at the position of the impurity. For an impurity adsorbed on a surface, this clearly

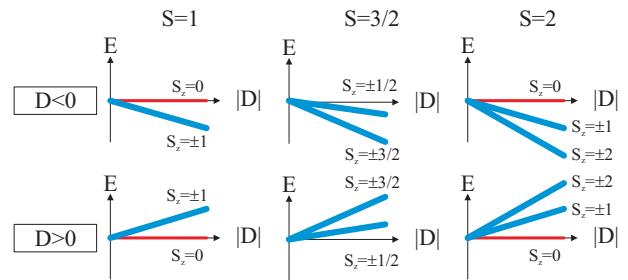


Figure 1: (Color online) Energy level diagrams for the anisotropic magnetic impurities with spin 1, 3/2 and 2 as a function of the absolute value of the anisotropy, $|D|$. Wide (blue) lines represent pairs of states, narrow (red) lines represent non-degenerate states.

cannot be a good approximation as the exchange interaction $J_{\mathbf{k},\mathbf{k}'}$ is inevitably anisotropic in the reciprocal space; nevertheless, since we focus mostly on the role of the local magnetic anisotropy terms, we will not pursue this issue in this work. We furthermore assumed that the exchange interaction is isotropic in the spin space.

In the anisotropy term of the Hamiltonian,

$$H_{\text{aniso}} = D S_z^2 + E (S_x^2 - S_y^2), \quad (4)$$

the first term is the *axial magnetic anisotropy*, while the second is named the *transverse magnetic anisotropy*. The axis z is by convention chosen such that $|D|$ is maximized, while axes xy are oriented so that $E > 0$. If the axial anisotropy term is negative, $D < 0$, we call the z axis an *easy axis*; if, however, $D > 0$ the anisotropy is said to be *hard-axis* (or planar). Axial anisotropy term D leads to the splitting of magnetic levels, Fig. 1. In the case of easy-axis anisotropy, $D < 0$, the moment tends to be maximal in size with two degenerate states pointing in the opposite directions, i.e. $S_z = \pm S$. Since the conduction band electrons can only change the impurity spin by one unit during a spin-flip scattering event, the exchange scattering rate is expected to be strongly reduced for large enough $|D|$. In the case of hard-axis anisotropy, $D > 0$, the single level $S_z = 0$ is favored for integer S and the doublet $S_z = \pm 1/2$ for half-integer S ; in both cases, the impurity moment will be compensated at low temperatures, since the doublet can be screened via the conventional spin-1/2 Kondo screening. It should be noted that $E(S_x^2 - S_y^2) = E/2 [(S^+)^2 + (S^-)^2]$ term, i.e. the transverse anisotropy, mixes levels with different values of S_z . This term, even when E is small, plays an essential role in the easy-axis case²⁸; in the hard-axis case, however, it only leads to a small correction.

The isotropic Kondo model (i.e. the $D = E = 0$ limit) has been intensively studied by a variety of techniques, such as numerical renormalization group^{32,33,34,35}, Bethe Ansatz^{36,37,38,39,40,41}, and other methods^{42,43,44}. These studies have uncovered the physics of *underscreening*: a single conduction channel can screen at most 1/2 unit of spin, so that at low temperatures the impurity remains magnetic with a residual spin of $S - 1/2$ ⁴⁵. It was found that for $S \geq 1$ the approach to the stable Fermi-liquid fixed point is slow (loga-

rithmic); this behavior was characterized as that of a singular Fermi liquid^{34,35}.

The anisotropic Kondo model with $D \neq 0$ (and with additional anisotropy in the exchange coupling) was studied by the Bethe-Ansatz technique^{46,47}. It was shown that anisotropy can induce a quantum critical point (i.e. non-Fermi-liquid behavior). The applicability of the Bethe-Ansatz approach is, however, limited to a set of models with restrained parameters thus a direct comparison with the model considered in this work is not possible. Nevertheless, there is qualitative agreement in that we also find a non-Fermi-liquid state for $D < 0$.

The anisotropic Kondo model was also previously studied by the numerical renormalization group technique in Refs. 28 and 29 with the focus on high values of spin S and easy-axis anisotropy as appropriate for molecular magnets (we note that the definition of D in the cited works differs in sign from ours). Where comparisons can be made, our results agree with theirs.

Finally, we mention that related models and physical effects are also studied in the context of transport spectroscopy of quantum dots and impurity clusters. The high conductance in the case of underscreening in spin-1 quantum dots and the two-stage Kondo screening were discussed in Refs. 48 and 49. Furthermore, the two-stage Kondo screening is also found in the case of a single conduction channel in multiple-quantum-dot structures, in particular in the case of side-coupled quantum dots^{50,51,52,53}. High-spin states can be obtained in systems of multiple impurities if the conduction-band-mediated exchange interaction is ferromagnetic^{54,55}, which may occur for small inter-impurity separations. Two-stage Kondo screening and the closely related ‘‘singlet-triplet’’ Kondo effect^{56,57,58,59,60,61} have both been intensively studied experimentally^{62,63,64,65,66,67}.

III. SCALING ANALYSIS

There is a close relation^{68,69} between the Kondo model with the DS_z^2 magnetic anisotropy term and the Kondo model with the XXZ anisotropic exchange constants J_z and J_\perp ^{69,70,71,72,73} defined by the Hamiltonian

$$H_K = J_z s_z S_z + J_\perp (s_x S_x + s_y S_y). \quad (5)$$

To be specific, we consider here the $S = 1$ anisotropic Kondo model with both types of the anisotropy (XXZ exchange and the DS_z^2 term, but $E = 0$). Taking into account that the energy of the $S_z = \pm 1$ intermediate states is higher by D as compared with the energy of the $S_z = 0$ state, the following scaling equations are obtained^{68,69,70}

$$\frac{dj_z}{dl} = \frac{1}{1-d} j_\perp^2, \quad (6)$$

$$\frac{dj_\perp}{dl} = \frac{1}{2} \left(1 + \frac{1}{1+d} \right) j_\perp j_z, \quad (7)$$

$$\frac{dd}{dl} = d - \ln 2 (j_z^2 - j_\perp^2). \quad (8)$$

Here the scaling parameter is $l = -\ln W$; it runs from 0 to positive infinity as the energy scale is reduced. Note that here

we denote the half-bandwidth by W (this departs from the NRG convention of denoting it by D). We have introduced dimensionless running coupling constants by absorbing the density of states ρ : $j_\perp = \rho J_\perp$, $j_z = \rho J_z$, while d is measured in the units of W : $d = D/W$. These scaling equations differ from those in Ref. 69 only by the d -dependent factors in Eqs. (6) and (7), which arise due to the energy shift by D in the $S_z = \pm 1$ states.

From Eq. (8) it follows that d will rapidly grow in absolute value⁶⁹, since the d term on the right hand side is first order, while the j_z^2 and j_\perp^2 terms are second order, hence smaller. The importance of the axial anisotropy is thus always reinforced at lower energy scales. Furthermore, starting from initially equal bare coupling constants, $j_z = j_\perp$, a non-zero d induces XXZ exchange anisotropy by unequal renormalization of j_z and j_\perp , as seen from Eqs. (6) and (7). At low energy scales, the physical properties are qualitatively the same irrespective of the origin of the anisotropy. From Eq. (8) we may also anticipate that the $D > 0$ case corresponds to a $J_\perp > J_z$ exchange anisotropic Kondo model, while the $D < 0$ case to a $J_\perp < J_z$ model⁶⁹.

IV. NUMERICAL RESULTS

Calculations were performed using the numerical renormalization group technique^{13,14,32,33,74,75} which consists of a logarithmic discretization of the continuum of states of the conduction band electrons, followed by mapping to a one-dimensional chain Hamiltonian with exponentially decreasing hopping constants. This Hamiltonian is then diagonalized iteratively by taking into account one new lattice site at each iteration. We have used discretization parameter $\Lambda = 2.5$ ($\Lambda = 2$ for spectral function calculations) and truncation with the energy cutoff at $E_{\text{cutoff}} = 10\omega_N$, where ω_N is the characteristic energy scale at the N -th iteration step. As a further precaution, truncation is always performed in a ‘‘gap’’ of width at least $0.01\omega_N$, so as not to introduce systematic errors. To prevent spurious polarization of the residual impurity spin in the $D < 0$ case due to floating-point round-off errors, it is helpful to symmetrize the energies of states which should be exactly degenerate (i.e. the $\pm S_z$ pairs). In all calculations, we have taken explicitly into account the conservation of charge Q ; in calculations with only the DS_z^2 anisotropy term ($E = 0$), a further conserved quantum number is S_z .

In all calculations we set $\rho J = 0.1$, therefore the Kondo temperature in the isotropic case, $T_K^{(0)}$, is the same for all values of spin S ^{37,44,54,76} and given by^{74,75}:

$$T_K^{(0)} \approx W \sqrt{\rho J} \exp\left(-\frac{1}{\rho J}\right) = 1.4 \times 10^{-5} W. \quad (9)$$

Extracting $T_K^{(0)}$ directly from the NRG results we obtain a more accurate value of $T_K^{(0)} = 1.16 \times 10^{-5} W$. (We use Wilson’s definition of the Kondo temperature^{37,74,77}.)

A. Static properties

We first consider the static (thermodynamic) properties, in particular the impurity contribution to the magnetic susceptibility, χ_{imp} , and the impurity contribution to the entropy, S_{imp} . The first quantity, when multiplied by the temperature, is a measure of the effective magnetic moment at a given temperature scale, while the second provides information about the effective impurity degrees of freedom.

In Fig. 2 we plot the thermodynamic properties of the anisotropic Kondo model with the axial DS_z^2 term ($E = 0$) for three different values of the impurity spin S and for a range of the anisotropy strength. As long as the temperature is larger than the anisotropy D , the curves follow closely the results for the isotropic case (black curves). At lower temperatures, the behavior of the system strongly depends on the sign of D . For negative D (easy-axis case), the impurity spin remains partially unscreened at low temperatures; for small $|D|$, the effective moment is slightly above the isotropic strong-coupling fixed-point value with spin $S - 1/2$ [i.e. $\mu = (S^2 - 1/4)/3$] and it saturates with increasing $|D|$ at the value of $\mu = S^2$. The low-temperature impurity entropy is $\ln 2$ for all negative D . This suggests that the impurity behaves as a residual two-level system with states $|+\rangle$ and $|-\rangle$, which in the large- $|D|$ limit become equal to the $|S_z = +S\rangle$ and $|S_z = -S\rangle$ states. The scattering of the low-energy electrons on this residual impurity states is discussed in App. A. For spin $S > 1$, the effective moment always increases as the temperature T is decreased below $|D|$, which reflects the progressive freezing out of the magnetic levels other than the maximally aligned $S_z = \pm S$ states. For spin 1, this is still the case for large enough $|D|$, but for lower $|D|$ the temperature dependence becomes monotonic. The boundary between the two different behaviors can be approximately located at $|D| \sim T_K^{(0)}$. The reason appears to be that for $|D| < T_K^{(0)}$, the $S = 1$ Kondo effect had already significantly screened the impurity spin yielding a residual spin $1/2$ by the time the anisotropy begins to be felt; the only effect of the anisotropy is then to prevent the screening process from completing, which gives a residual spin value slightly above $1/2$.

For positive D (hard-axis case), the impurity is non-magnetic at low temperatures for any value of the impurity spin S . Unlike in the easy-axis case, we see a larger variety of possible behaviors in the approach to the fixed point depending on the spin and on the anisotropy strength. We discuss $S = 3/2$ and $S = 2$ first; these are characteristic representatives for all half-integer and integer spin cases.

For half-integer spin and small $D < T_K^{(0)}$, the curves just follow the results for the isotropic case until $T \sim D$, when spin states other than the $S_z = 0$ state of the residual (integer!) $S - 1/2$ impurity spin freeze out and the system approaches the non-magnetic ground state exponentially fast. For sufficiently large $D > T_K^{(0)}$, the high $|S_z|$ states of the original impurity spin freeze out exponentially fast at $T \sim D$, this time yielding a $S_z = \pm 1/2$ doublet which then undergoes spin- $1/2$ Kondo screening. It must be stressed, however, that after the high- $|S_z|$ states are frozen out, the effec-

tive model in the restrained $S_z = \pm 1/2$ subspace does *not* correspond to an isotropic spin- $1/2$ model, but rather to an exchange anisotropic spin- $1/2$ model with

$$J_{\perp} \approx 2J, \quad J_z \approx J. \quad (10)$$

The mapping on an anisotropic Kondo model stems from the spin- $3/2$ operators which are given in the matrix notation as

$$S_x = \begin{pmatrix} 0 & \frac{\sqrt{3}}{2} & 0 & 0 \\ \frac{\sqrt{3}}{2} & 0 & 1 & 0 \\ 0 & 1 & 0 & \frac{\sqrt{3}}{2} \\ 0 & 0 & \frac{\sqrt{3}}{2} & 0 \end{pmatrix}, \quad (11)$$

$$S_z = \begin{pmatrix} \frac{3}{2} & 0 & 0 & 0 \\ 0 & \frac{1}{2} & 0 & 0 \\ 0 & 0 & -\frac{1}{2} & 0 \\ 0 & 0 & 0 & -\frac{3}{2} \end{pmatrix}.$$

In the $S_z = \pm 1/2$ subspace, S_z yields $\frac{1}{2}\sigma_z$, while $S_{x,y}$ yield $2 \times \frac{1}{2}\sigma_{x,y}$, i.e. twice the spin- $1/2$ operators in the transverse directions. The Kondo temperature is thus given by the expression for the XXZ anisotropic Kondo model:

$$T_K \approx W \exp\left(-\frac{\alpha}{\rho J_z}\right),$$

$$\alpha = \frac{\arctan \gamma}{\gamma}, \quad (12)$$

$$\gamma = \sqrt{\left(\frac{J_{\perp}}{J_z}\right)^2 - 1}, \quad \text{for } J_{\perp} \geq J_z,$$

which can be derived from the scaling equations to second order²⁸. For reference we also note that the expression for $J_{\perp} < J_z$ can be obtained by analytic continuation, giving

$$T_K \approx W \exp\left(-\frac{\alpha}{\rho J_z}\right),$$

$$\alpha = \frac{\operatorname{arctanh} \gamma}{\gamma}, \quad (13)$$

$$\gamma = \sqrt{1 - \left(\frac{J_{\perp}}{J_z}\right)^2}, \quad \text{for } J_{\perp} \leq J_z.$$

These expressions somewhat overestimate the true Kondo temperature since they do not include the $\sqrt{\rho J_z}$ factors; numerically calculated Kondo temperatures are shown in Fig. 3.

The value of the Kondo temperature of the effective spin- $1/2$ screening process depends on D and it can exceed $T_K^{(0)}$ since $\alpha < 1$ in the transverse dominated $J_{\perp}/J_z > 0$ case; in the infinite- D limit, $T_K(S = 1/2)$ goes to

$$T_K(S = 1/2) \approx 9 \times 10^{-4} W. \quad (14)$$

This result fully agrees with T_K in the exchange-anisotropic Kondo model, Fig. 3. For finite D , the effective ratio J_{\perp}/J_z may be different from 2, since there is a temperature range where the $S_z = \pm 3/2$ levels still affect the renormalization of the exchange interaction before they completely freeze

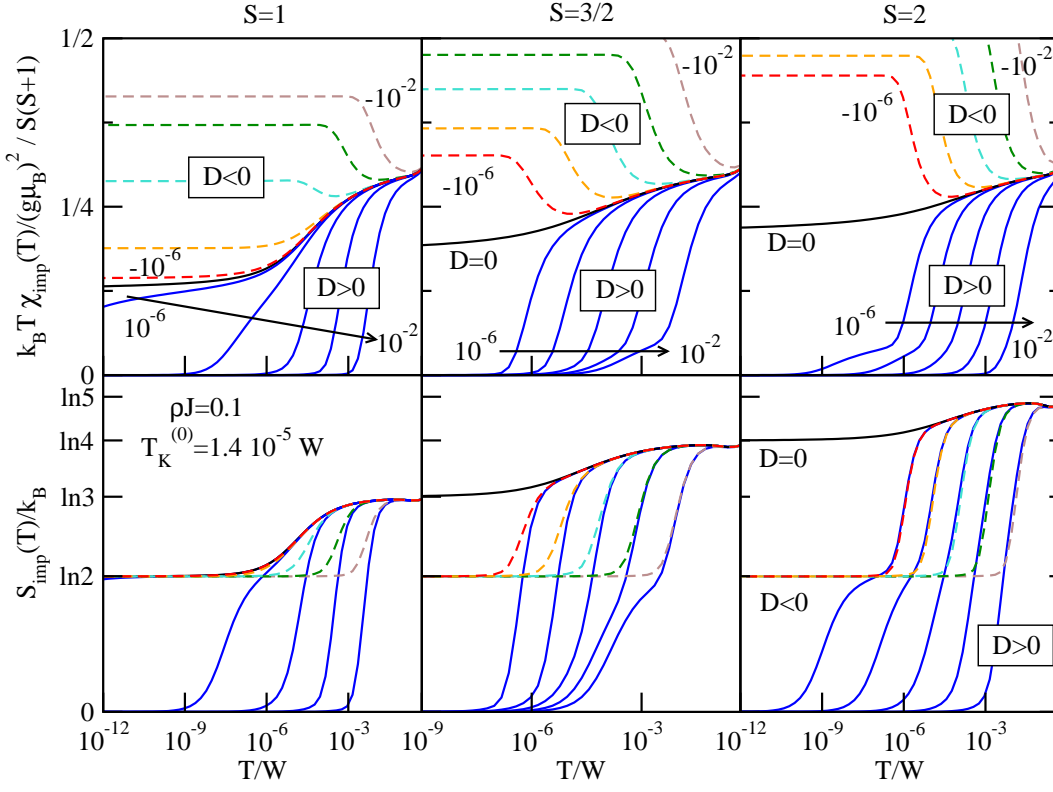


Figure 2: (Color online) Thermodynamic properties of the anisotropic Kondo model. We plot the impurity contribution to the magnetic susceptibility, χ_{imp} , and the impurity contribution to the entropy, S_{imp} . Full (blue) lines correspond to positive anisotropy, $D > 0$, dashed (red) lines correspond to negative anisotropy, $D < 0$, while black line is the isotropic case, $D = 0$. The arrow indicate in which direction the anisotropy is increasing. Note that the vertical axis in the upper panels is additionally rescaled as $1/S(S+1)$.

out. The intrinsic anisotropy of the effective spin-1/2 Kondo model also plays a role in the splitting (shifting) of the Kondo resonance in a magnetic field: for strong magnetic field B_z in the z -direction, we expect a shift of $\sim g\mu_B B_z$, and a shift approximately twice as large for fields in the transverse directions²⁵. Finally, we note that for larger spin values we have $J_{\perp} = 3J$ (spin 5/2), $J_{\perp} = 4J$ (spin 7/2), and in general

$$J_{\perp} = (S + 1/2)J. \quad (15)$$

For integer $S \geq 2$, the situation is the opposite. Now the regime of the exponential approach to the $S_z = 0$ ground state corresponds to $D > T_K^{(0)}$. For $D < T_K^{(0)}$, on the other hand, the low-temperature behavior is again that of the spin-1/2 Kondo model. This is made possible by the combined effect of the spin- S Kondo screening at higher temperatures giving rise to the $S - 1/2$ (i.e. half-integer) residual impurity spin, and of the axial anisotropy which leads to freezing out of the high-spin $S_z = \pm(S - 1/2), \dots, \pm 3/2$ levels of this residual object to finally give rise to a residual spin-1/2 object. This residual spin-1/2 then finally undergoes a spin-1/2 Kondo screening. At first sight it might even seem surprising that the residual spin is compensated at all, given that in the isotropic high-spin Kondo model the residual exchange interaction is ferromagnetic, yet for $D > 0$ the induced exchange anisotropy (see Sec. III) is of the type which leads to

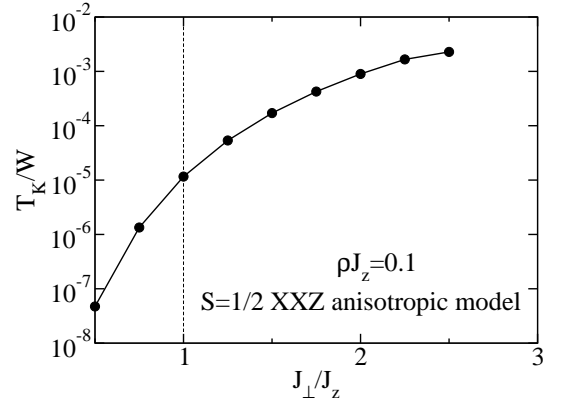


Figure 3: The Kondo temperature of the XXZ anisotropic $S = 1/2$ Kondo model as a function of the J_{\perp}/J_z ratio.

complete screening of the impurity spin⁶⁸. Since the residual $(S - 1/2)$ spin is an extended object, there is no simple mapping on the effective spin-1/2 Kondo model and it appears difficult to estimate the effective exchange constants J_{\perp} and J_z even in the $D \rightarrow 0$ limit. The effective bandwidth on the other hand is clearly given by $W_{\text{eff}} = \alpha D$, where α is some constant of order 1. The Kondo temperature is thus given by $T_K(S = 1/2) \approx Df(D)$, where $f(D)$ turns out to be a

power-law function with non-integer exponent, $f(D) \sim D^{1.3}$ for $S = 2$ and $f(D) \sim D^{0.7}$ for $S = 3$. see Fig. 4. For large spin t

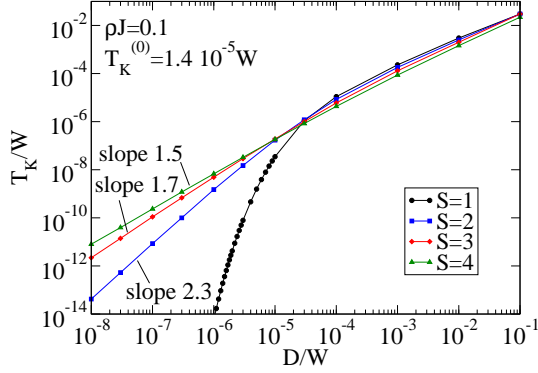


Figure 4: (Color online) The cross-over temperature (identified with the spin-1/2 Kondo temperature T_K for $D < T_K^{(0)}$) in integer-spin anisotropic Kondo models for the hard-axis case.

We would like to emphasize the important fact that the original impurity spin S and the residual spin $S - 1/2$ after the Kondo screening belong to different classes (one is integer, the other half-integer). For this reason we always find different behavior depending on which of the D and $T_K^{(0)}$ is smaller. Furthermore, this explains similarities between integer S for $D < T_K^{(0)}$ and half-integer S for $D > T_K^{(0)}$.

Finally we consider the special case of integer spin 1. For large $D > T_K^{(0)}$, the behavior is the same as for other integer spins. For small $D < T_K^{(0)}$, the approach to the strong-coupling fixed point is of the spin-1/2 Kondo model type. However, we find that the second Kondo temperature $T_K^{(2)}$ depends exponentially on the $D/T_K^{(0)}$ ratio, see Fig. 4, a situation strongly reminiscent of the two-stage Kondo screening⁷⁸ in the side-coupled impurity systems^{50,51,52,53,79}. At $T_K^{(0)}$ the spin is screened from $S = 1$ to $S = 1/2$ by the spin-1 Kondo effect, then at $T_K^{(2)}$ from $S = 1/2$ to $S = 0$ by the spin-1/2 Kondo effect. It is possible to fit the results with

$$T_K^{(2)} = \alpha T_K^{(0)} e^{-\gamma \frac{T_K^{(0)}}{J_{\text{eff}}}} \quad (16)$$

where

$$J_{\text{eff}} = D + c T_K^{(0)} \quad (17)$$

with coefficients $\alpha = 0.052$, $\gamma = 2.531$, $c = 0.0661$. This fit is only of phenomenological value: the situation here is different from the one in the side-coupled impurity case, where it is possible to interpret the results in terms of screening of the second impurity by the quasiparticles resulting from the first stage of the Kondo screening and where J_{eff} corresponds to real exchange coupling.

In Fig. 5 we plot the thermodynamic quantities for the related $S = 1$ Kondo model with XXZ exchange anisotropy⁶⁹. As expected, we find that $J_{\perp} < J_z$ models behave similarly to $D < 0$, and $J_{\perp} > J_z$ similarly to $D > 0$. In the presence

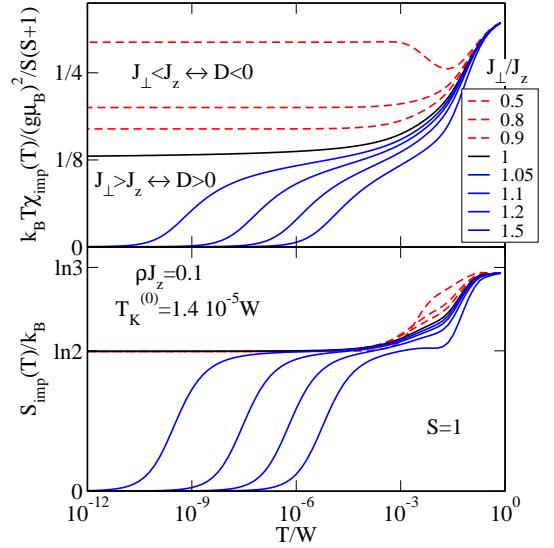


Figure 5: (Color online) Thermodynamic properties of the $S = 1$ Kondo model with XXZ exchange anisotropy.

of both symmetries, the two anisotropies may either enhance each other or compete.

In Fig. 6 we plot the impurity contribution to the entropy for the fully anisotropic problem with the DS_z^2 and $E(S_x^2 - S_y^2)$ terms (impurity contribution to the magnetic susceptibility cannot be easily computed since S_z is no longer a good quantum number). We consider both the case when E is large [subfigure a) with $E = 0.2|D|$]; such ratio is found, for example, for integer spin-2 Fe impurities on CuN/Cu surfaces where $D = -1.5$ meV and $E = 0.3$ meV, and for half-integer spin-5/2 Mn impurities on the same surface¹⁰] and for the case where E is much lower than $|D|$ [subfigure b) with $E = 0.01|D|$]; no such magnetic adatom/surface system had been identified so far in the negative- D systems, but E appears to be much smaller than D in the positive- D Co on CuN/Cu system].

The ground state for $E \neq 0$ is non-degenerate for all parameters. For $D > 0$, the $S_x^2 - S_y^2$ operator is an irrelevant perturbation and the thermodynamic behavior of the system is hardly affected. For $D < 0$, however, the perturbation is relevant and drives the system to a different, non-magnetic ground state for all S . For $S = 1$, the degeneracy is lifted on the scale of E if $E > T_K^{(0)}$; for $E < T_K^{(0)}$ there appears to be Kondo-like screening of the residual spin-1/2 with exponential reduction of the second Kondo temperature, similar to what happens in the $D > 0$ case. Thus the E -term can induce two-stage Kondo behavior even in the $D < 0$ case. For half-spin $S = 3/2$, the degeneracy is again lifted on the scale of E if $E < T_K^{(0)}$. If $E > T_K^{(0)}$, previously known Kondo effect with pseudo-spin 1/2 occurs²⁸; the Kondo temperature depends on parameters in a non-trivial way. For integer spin $S = 2$, we find degeneracy lifting on the scale of E if $E > T_K^{(0)}$, and a pseudo-spin 1/2 Kondo effect if $E < T_K^{(0)}$. The effective bandwidth is now given by $W_{\text{eff}} = \alpha E$, where α is some constant of order 1, so the Kondo temperature is

given by $T_K \approx Ef(D, E)$ where $f(D, E)$ has power-law behavior as a function of D with a D/E (and spin S) dependent exponent, see Fig. 7.

We conclude that the easy-axis systems with transverse anisotropy behave rather similarly to hard-axis systems; in the conditions for the emergence of the pseudo-spin $S = 1/2$ Kondo effect the quantity E takes the place of D .

B. Properties of the $D < 0$ systems

For any $S \geq 1$ and $D < 0$, $E = 0$, the ground state is twofold degenerate. The fixed-point spectra depend on the value of D , thus the S_z^2 term is a marginal operator. At low temperatures, these systems have a Curie-like magnetic response with fractional spin

$$\chi_{\text{imp}}(T \rightarrow 0) = (g\mu_B)^2 \frac{\mathcal{C}(D)}{k_B T}. \quad (18)$$

This is reminiscent of the fractional-spin non-Fermi-liquid fixed points in the pseudo-gap Kondo model with $\rho(\omega) \sim |\omega|^r$ density of states for spin 1 and $r > 0^{80,81,82,83}$ and in the related power-law Kondo model in the case of ferromagnetic coupling and $r < 0^{84}$. There are nevertheless some notable differences. The fixed points in the pseudo-gap Kondo model are found to be unstable with respect to the particle-hole symmetry breaking. The fixed points we find are, however, stable with respect to particle-hole symmetry breaking: both anisotropy, S_z^2 , and potential scattering, n_{f_0} , are marginal operators. Furthermore, the fixed point in the anisotropic Kondo model has entropy $\ln 2$ (i.e. impurity behaves as a two-level system), while the fixed point in the pseudo-gap Kondo model has entropy $(1 + 2r) \ln 2^{80,81}$.

In Fig. 8 we plot the Curie constant as a function of the $D/T_K^{(0)}$ ratio. The transition from the isotropic limit

$$\mathcal{C} = (S - 1/2)(S + 1/2)/3 = (S^2 - 1/4)/3, \quad (19)$$

to the saturated easy-axis anisotropic behavior,

$$\mathcal{C} = S^2, \quad (20)$$

is approximately logarithmic, i.e. very slow. This reflects the underlying underscreened Kondo effect and the partial screening of the impurity moment which also feature similarly slow logarithmic dependence of the magnetic susceptibility on temperature and magnetic field.

In Fig. 9 we plot the energy levels of the spin-1 negative- D model as a function of the anisotropy D . For small $|D|$, the levels approach the free electron spectrum with $\pi/2$ phase shift (which is due to the Kondo effect) with additional two-fold degeneracy of all levels due to the decoupled spin-1/2 residual impurity spin. For large $|D|$, the levels tend towards a spectrum with states clustered near the energies of the free electron spectrum with zero phase shift (no Kondo effect) with additional splitting due to residual anisotropic exchange coupling that will be studied in App. A. For intermediate $|D|$, the spectrum is more complex. It can be characterized as free

electron spectrum with some intermediate phase shift with additional splitting due to residual exchange interaction; as $|D|$ is swept from 0 to $+\infty$, the (spin-dependent) phase shift is reduced from $\pi/2$ to 0, while the nature of the residual impurity spin changes from isotropic spin-1/2 doublet to the anisotropic $S_z = \pm 1$ magnetic doublet, and the residual exchange constants increase from 0 to some finite value of the order of the bare exchange coupling J , see also App. A.

C. Dynamic properties

To characterize dynamic properties of the anisotropic models, we calculate the T-matrix and the dynamical spin susceptibility^{85,86,87,88}. The T-matrix for the Kondo model can be determined by computing the Green's function^{35,89,90}

$$G(\omega) = \langle\langle S^- f_{0\downarrow} + S^z f_{0\uparrow}; S^+ f_{0\downarrow}^\dagger + S^z f_{0\uparrow}^\dagger \rangle\rangle_\omega, \quad (21)$$

where $S^\pm = S_x \pm iS_y$ are the impurity spin operators and $f_{0\sigma}^\dagger$ creates an electron with spin σ on the first site of the hopping Hamiltonian^{14,74}. Assuming constant exchange constant $J_{\mathbf{k},\mathbf{k}'} \equiv J$, the T-matrix is then given by

$$T(\omega) = J^2 G(\omega). \quad (22)$$

This quantity contains information on both elastic and inelastic scattering rate (cross section)^{35,90,91}:

$$\begin{aligned} \sigma_{\text{total}}(\omega)/\sigma_0 &= \rho\pi^2 \left(-\frac{1}{\pi} \text{Im}T(\omega) \right), \\ \sigma_{\text{el}}(\omega)/\sigma_0 &= \rho^2 \pi^2 |T(\omega)|^2, \\ \sigma_{\text{inel}}(\omega) &= \sigma_{\text{total}}(\omega) - \sigma_{\text{el}}(\omega), \end{aligned} \quad (23)$$

where σ_0 is the scattering rate in the case of unitary scattering³⁵. These scattering rates can, in turn, be related to the amplitude of the impurity-related spectral features in scanning tunneling spectroscopy experiments^{20,21,92,93}, thus in the following we will call the quantity $\sigma_{\text{total}}(\omega)$ the ‘‘conductance’’ and we will express it in the units of σ_0 . We also note that the zero-temperature scattering rate in a Fermi-liquid system is

$$\sigma_{\text{total}}(\omega \rightarrow 0) = \sigma_{\text{el}}(\omega \rightarrow 0) = \sigma_0 \sin^2(\delta), \quad (24)$$

where δ is the quasiparticle scattering phase shift, while $\sigma_{\text{inel}}(\omega \rightarrow 0) = 0$.

The imaginary part of the dynamical spin susceptibility $\mathcal{S}_{\alpha\alpha}(\omega)$ (with $\alpha = x, y, z$) is defined as

$$\mathcal{S}_{\alpha\alpha}(\omega) = -\frac{1}{\pi} \text{Im} \langle\langle S_\alpha; S_\alpha \rangle\rangle_\omega. \quad (25)$$

The dynamical spin susceptibility is in principle observable in tunneling-current-noise spectroscopy using spin-polarized STM^{94,95}. Our results thus provide information on how the Kondo effect in the presence of magnetic anisotropy modifies the current noise. In addition, the dynamical spin susceptibility contains information on the differential cross section

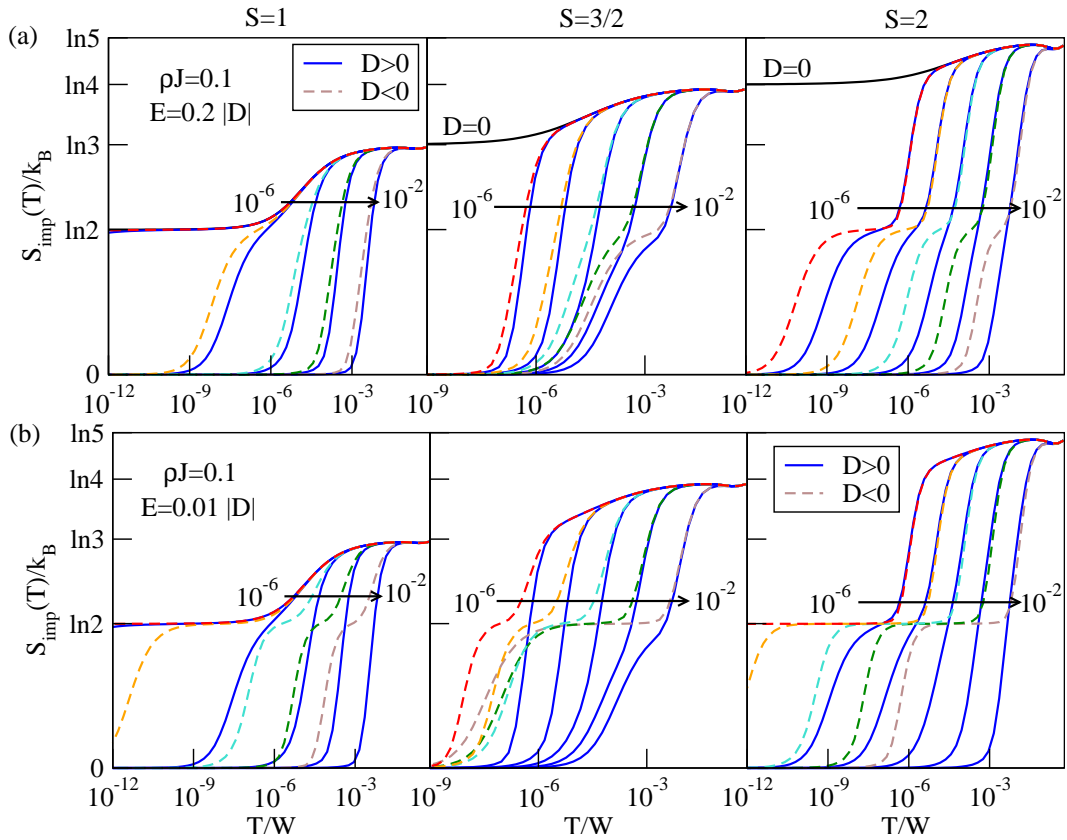


Figure 6: (Color online) Impurity contribution to the entropy of the anisotropic Kondo model with $DS_z^2 + E(S_x^2 - S_y^2)$ terms with constant ratio (a) $E/|D| = 0.2$ and (b) $E/|D| = 0.01$. We plot $D = 10^{-6}, 10^{-5}, \dots, 10^{-2}$; the arrow indicate in which direction the anisotropy is increasing.

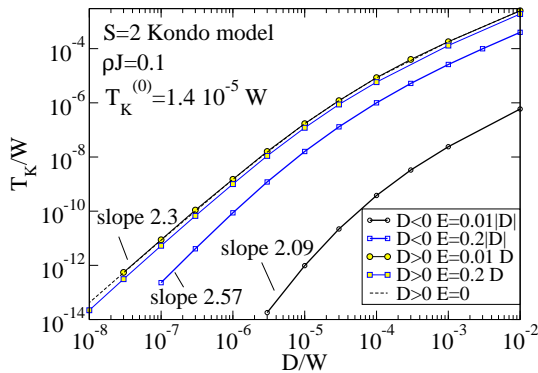


Figure 7: (Color online) The cross-over temperature (identified with the spin-1/2 Kondo temperature T_K for $D < T_K^{(0)}$) in the $S = 2$ anisotropic Kondo model with transverse anisotropy.

$\sigma(\omega, \Delta)$, where Δ is the energy exchange⁹⁶; the differential cross sections is also possibly measurable⁹⁶.

In Fig. 10 we plot the dynamic properties of the anisotropic Kondo model with the DS_z^2 term ($E = 0$). We discuss first the conductance. In the isotropic $D = 0$ case, the conductance always rises to the unitary limit, albeit the approach to this limit is slow (logarithmic)^{34,35,43,48}. Unitary scattering can

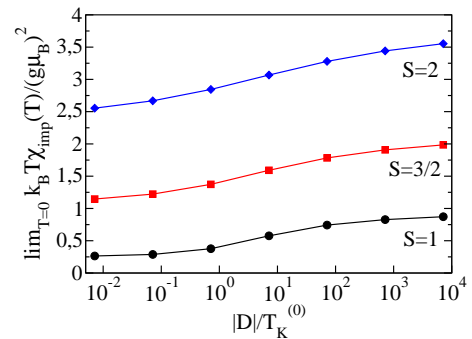


Figure 8: (Color online) Curie constant as a function of the $|D|/T_K^{(0)}$ ratio for $S = 1, 3/2, 2$ Kondo models with easy-axis anisotropy, $D < 0$.

be explained by the well known fact that in the isotropic case a single conduction channel screens precisely 1/2 unit of the impurity spin and, in doing so, the low-energy conduction band electrons gather a $\pi/2$ scattering phase shift.

In the hard-axis $D > 0$ case, the conductance at low temperatures is zero for all integer values of the impurity spin, while it is unitary for all half-integer spins. For $S = 1$ and $D < T_K^{(0)}$, this can be explained by the two-stage Kondo screening: the first $S = 1$ screening stage leads to increased

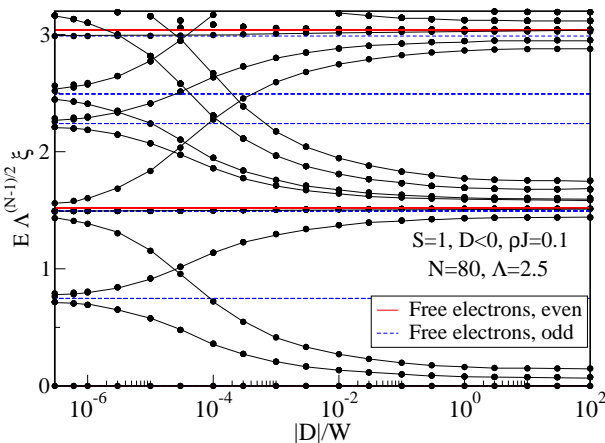


Figure 9: (Color online) Energy levels at iteration $N = 80$ ($T \sim 10^{-16}W$) as a function of the anisotropy D in the spin-1 Kondo model with easy-axis anisotropy, $D < 0$.

conductance as in the isotropic case, however the conductance drops to zero at a lower temperature scale $T_K^{(2)}$ when the residual spin-1/2 is compensated in the second screening stage. This is similar to the screening of a $S = 1$ impurity by two conduction channels with unequal exchange constants^{42,63}, but here the two-stage screening occurs with a single channel. Non-monotonous energy-dependence of the spectral function is also found in the case of side-coupled impurities, but there both screening stages are of the $S = 1/2$ kind^{50,51,52,53}. For large $D > T_K^{(0)}$, the anisotropy makes the impurity non-magnetic, there is no exchange scattering at energy scales below D and the low-temperature conductance drops to zero. Note that in both cases the stable fixed point is the same, the ratio $D/T_K^{(0)}$ merely determines by which mechanism the $S = 1$ Kondo screening is interrupted by the anisotropy; the transition between the two regimes is smooth.

For higher integer spins (represented in Fig. 10 by the $S = 2$ case), the situation is in some respect similar. For $D < T_K^{(0)}$, the conductance at first increases during the initial spin- S Kondo screening, there is even a slight bump above the result for the isotropic case on the energy scale of D when the effective spin doublet is formed and there is additional resonantly enhanced scattering. Spin- S Kondo screening yields a half-integer effective impurity spin, thus a spin-1/2 doublet on the energy scale D . The spin-1/2 Kondo screening then leads to a decrease in conductance to zero. As previously discussed, the main difference from the $S = 1$ case is that there is no exponential reduction of the energy scale for $D < T_K^{(0)}$.

For half-integer spins (represented in Fig. 10 by the $S = 3/2$ case), the conductance at low temperatures is unitary, as in the isotropic case. For $D > T_K^{(0)}$, this may be explained by the fact that the anisotropy leads in this case to a low-laying doublet formed by the $S_z = \pm 1/2$ magnetic doublet which undergoes Kondo screening like in the conventional spin-1/2 Kondo model. The doublet is formed before the spin- S Kondo screening commences and the mapping to the spin-1/2 Kondo model is a good approximation: the Kondo resonance then has

approximately Lorentzian form. It may be noted that there is again an additional peak in $\sigma(\omega)$ at $\omega \sim D$ due to resonantly enhanced scattering by the $S_z \rightarrow S_z \pm 1$ processes. For $D < T_K^{(0)}$, the conductance curve first follows the logarithmically increasing isotropic spin- S curve, then at D the approach to the unitary limit becomes faster.

We emphasize the marked difference between the integer spin $S = 2$ and the half-integer spin $S = 3/2$ regarding the energy scale where the limiting value of σ_{total} (0 viz. 1) is approached: for $S = 2$, the characteristic frequency decreases faster than linearly with D for small D , while for $S = 3/2$ it tends to increase very slowly with D for large D . In both cases this behavior is due to the underlying effective $S = 1/2$ Kondo physics; for $S = 2$ it implies that the effective exchange constant becomes smaller as D is reduced, while for $S = 3/2$ this is due to the saturation of the effective J_{\perp}/J_z ratio for large D as already discussed.

We now consider the easy-axis $D < 0$ case. For all S , the conductance is found to saturate at some D -dependent finite value here. This reflects the presence of a residual uncompensated impurity spin which induces scattering at low temperatures which is neither unitary nor zero (these are the only two possibilities compatible with a Fermi-liquid system in the presence of the particle-hole symmetry which imposes the restriction $\delta \equiv -\delta \pmod{\pi}$ on the quasiparticle scattering phase shift δ , thus $\delta = 0$ or $\delta = \pi$). This implies that the stable fixed point may be classified as a non-Fermi liquid, which is confirmed by the non-vanishing inelastic scattering rate at the Fermi level, see Fig. 11. In the limit $|D| \rightarrow 0$, this non-Fermi-liquid fixed point evolves continuously into a singular Fermi-liquid fixed point of the isotropic underscreened Kondo model. Since the approach to this limit is slow (in particular for $S \geq 3/2$), even very small negative axial anisotropy will lead to significantly reduced conductance at low temperatures. In the following we show that this behavior is modified by non-zero E (see also Ref. 28). Nevertheless, if $E \ll |D|$, there might exist a temperature range where the non-Fermi-liquid behaviour is observable.

We now consider the imaginary part of the dynamic spin susceptibility $\mathcal{S}_{\alpha\alpha}(\omega)$. We recall that these quantities are given at zero temperature by

$$\mathcal{S}_{\alpha\alpha}(\omega) = -\frac{1}{\pi} \frac{1}{Z_N} \sum_{i,j_{\text{GS}}} | \langle i | S_{\alpha} | j_{\text{GS}} \rangle |^2 \delta(\omega - (E_i - E_{\text{GS}})) \quad (26)$$

where the index i runs over the excited states and the index j_{GS} over the degeneracy of the ground state, while Z_N is the zero-temperature partition function (equal to the degeneracy of the ground state). In the absence of the coupling to the conduction band, the transverse susceptibility $\mathcal{S}_{xx}(\omega)$ features delta peak(s) at

$$\omega = |DS_x^2 - D(S_z - 1)^2| = |D(2S_z - 1)|, \quad (27)$$

since S_x couples neighboring levels. For $S = 1$, there is thus a peak at $|D|$, for $S = 3/2$ a peak at $2|D|$ and for $S = 2$, depending on the sign of D , a peak at D (for $D > 0$) or at $3|D|$ (for $D < 0$). The longitudinal susceptibility $\mathcal{S}_{zz}(\omega)$ of a decoupled impurity is zero.

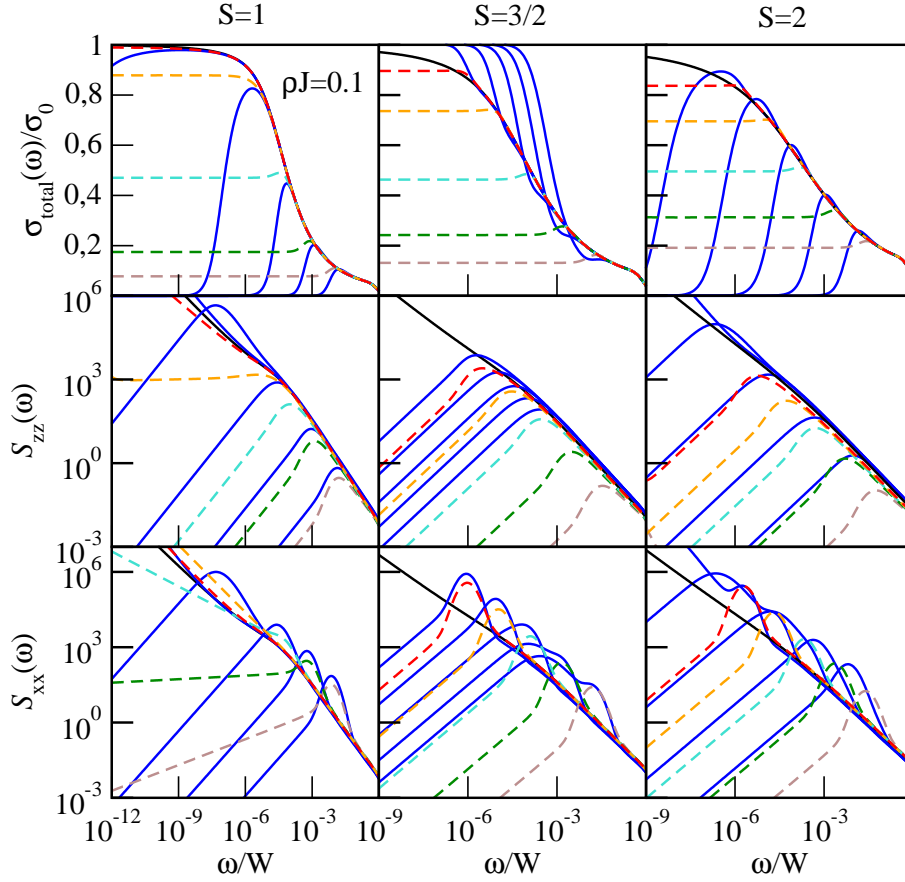


Figure 10: (Color online) Dynamic properties of the anisotropic Kondo model. We plot the spectral function of the T -matrix (“conductance”) and the longitudinal and transversal dynamical susceptibility $\mathcal{S}_{zz}(\omega)$ and $\mathcal{S}_{xx}(\omega)$. The curves correspond to $|D| = 10^{-2}, \dots, 10^{-6}$; the curve styles are the same as in Fig. 2. Note that for $S = 2$ and $D = 10^{-6}$ the susceptibility curves do not diverge; they start decreasing at an energy scale outside the displayed range.

The $S = 1$ case has some special features, so we focus first on the regular cases, $S \geq 3/2$. The longitudinal susceptibility $\mathcal{S}_{zz}(\omega)$ always has a single peak. In the hard-axis $D > 0$ case we find that the peak occurs at the energy scale of the effective $S = 1/2$ Kondo effect (when it occurs, i.e. $D > T_K^{(0)}$ for $S = 3/2$ and $D < T_K^{(0)}$ for $S = 2$, respectively) or at $\sim D$ in the regime with no $S = 1/2$ Kondo effect. In both cases this corresponds to the energy scale where the conductance approaches its limiting value, as discussed above. This result is expected, since in the presence of the Kondo effect the largest magnetic fluctuations always occur on the energy scale of T_K , which is a reflection of the anomalously strong spin-flip scattering of the conduction band electrons off the impurity; in the absence of the Kondo effect, magnetic fluctuations occur on the scale of the local magnetic excitation energy, in this case the anisotropy D . In the easy-axis $D < 0$ case, the position of the peak in $\mathcal{S}_{zz}(\omega)$ is always $\sim |D|$.

For all D and all $S \geq 3/2$, the approach to the zero frequency limit is linear, while the behavior at high frequencies is described approximately by a power law $\mathcal{S}(\omega) \sim \omega^{-\gamma}$ with exponents γ that are slightly above 1⁷³.

The transverse susceptibility $\mathcal{S}_{xx}(\omega)$ is more complex. In

the hard-axis $D > 0$ case, we find a two-peak behavior in the parameter regime with $S = 1/2$ Kondo effect: the first peak corresponds to the scale of D , the second to the scale of T_K . In the transition regime $D \sim T_K^{(0)}$, the two peaks merge into a single peak which then follows the scale of anisotropy D . In the easy-axis $D < 0$ case, the curves again have a single peak at $\sim |D|$. At this point a comment on the peak width is in order: the peaks at $\sim |D|$ are over-broadened due to the broadening procedure used in the NRG method, thus the very narrow peaks take the form of the broadening kernel⁹⁶.

We now finally turn to $S = 1$. For hard-axis $D > 0$ anisotropy, we find for both $\mathcal{S}_{zz}(\omega)$ and $\mathcal{S}_{xx}(\omega)$ a single peak centered at $\omega \sim D$ (for $D > T_K^{(0)}$) or at $\omega \sim T_K^{(2)}$ (for $D < T_K^{(0)}$). In $\mathcal{S}_{xx}(\omega)$, there is no additional peak on the scale of D for $D < T_K^{(0)}$, as was the case for the spin-2 model, but we observe a change of slope at $\omega \sim T_K^{(0)}$. Even more peculiar are the results for the easy-axis $D < 0$ case. The longitudinal susceptibility has a linear frequency dependence for $|D| \gtrsim T_K^{(0)}$, but for $|D| \lesssim T_K^{(0)}$ we observe ω^α scaling with exponent α which depends on the anisotropy D and which turns negative approximately at $|D| \sim T_K^{(0)}$, i.e. the suscep-

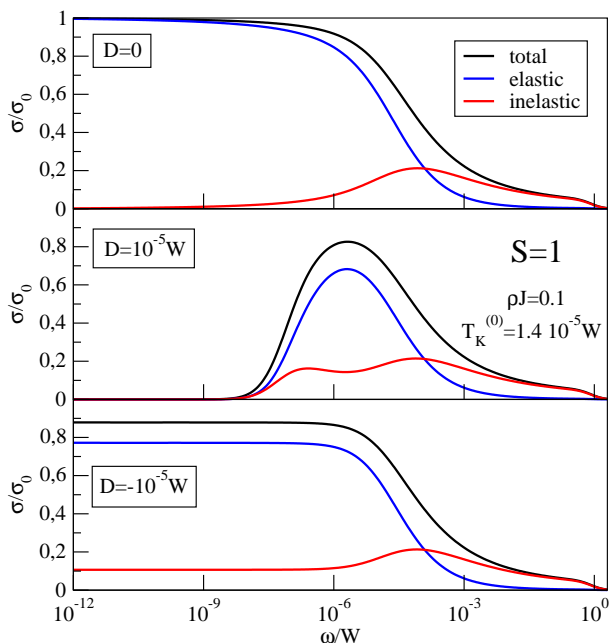


Figure 11: (Color online) Total, elastic and inelastic scattering cross sections for the $S = 1$ Kondo model with no anisotropy, positive anisotropy and negative anisotropy.

tibility becomes divergent. In the transverse susceptibility we find a strong deviation from linear scaling for all values of $|D|$, with divergent behavior already for $|D|$ much larger than $T_K^{(0)}$. We emphasize that for all spin values S , the easy-axis $D < 0$ systems exhibit non-Fermi-liquid features (such as finite inelastic scattering at $\omega = 0$), but only for $S = 1$ is the dynamic spin susceptibility divergent at low frequencies.

We note that a linear frequency dependence of $S_{\alpha\alpha}(\omega)$ at low frequencies must hold in Fermi-liquid systems as mandated by the Korringa-Shiba relations^{72,96,97,98}. For $D < 0$ the system is, however, non-Fermi liquid and the static magnetic susceptibility is diverging for all S , thus $S(\omega)$ is not expected to be linear. We view the fact that it is linear for $S \geq 3/2$ merely as a coincidence.

We finish our discussion of dynamic properties by showing that in the presence of the transverse anisotropy term $E(S_x^2 - S_y^2)$, all non-Fermi-liquid features disappear, Fig. 11. In particular, we observe that for all integer S the low-temperature conductance is zero, while for all half-integer S it is unitary, irrespective of the sign and size of the axial anisotropy D . Furthermore, the spin susceptibility always has linear frequency dependence at low frequencies. This agrees with the results for static properties.

V. CONCLUSION

Due to the presence of the magnetic anisotropy, the impurity spin is always completely compensated at low enough temperature, even in the case of high-spin impurities coupled to a single continuum channel. This goes against the common

wisdom that a single channel can screen at most $1/2$ unit of spin, which results in a residual spin of $S - k/2$ in the case of k screening channels: such a behavior will only be observable for isotropic systems, a situation which is rather unlikely for magnetic impurities adsorbed on surfaces.

The approach to the fully screened impurity spin with decreasing energy scale depends on the impurity spin S , the sign of axial anisotropy D , and on the hierarchy of the energy scales, in particular on the dichotomy $D < T_K^{(0)}$ or $D > T_K^{(0)}$ in the positive- D models. For positive D (hard-axis case), we find spin- $1/2$ Kondo screening at low temperatures in the weak-anisotropy case $D < T_K^{(0)}$ for integer spin (with exponentially reduced Kondo temperature in the special case of spin 1) and in the strong-anisotropy case $D > T_K^{(0)}$ for half-integer spin; in other cases, the effective impurity moment drops to zero exponentially on the energy scale of D . The transverse anisotropy E does not play an important role for $D > 0$. For negative D (easy-axis case), however, it changes the behavior of the system completely. For $E = 0$, the impurity spin would be only partially screened, leading to residual spin-dependent scattering and non-Fermi-liquid behavior. In real systems $E \neq 0$ and the behavior of $D < 0$ becomes similar to that of the $D > 0$ systems: for $S = 1$ we again find two-stage Kondo screening for $E < T_K^{(0)}$, for $S = 3/2$ there is effective spin- $1/2$ Kondo effect for $E > T_K^{(0)}$, while for $S = 2$ we find effective spin- $1/2$ screening for $E < T_K^{(0)}$. If $E \ll |D|$, some features of the non-Fermi-liquid behavior might be observable in intermediate temperature respectively energy regimes. The zero-temperature conductance is found to be zero for all integer spins and unitary for all half-integer spins for both signs of D (assuming $E \neq 0$). For integer spin and $E, D < T_K^{(0)}$, the temperature dependence of the conductance is expected to be non-monotonous with increased conductance in the $T_K(S = 1/2) < T < T_K^{(0)}$ range. The most likely candidate for observation of underscreening is the $S = 1$ case due to the exponential reduction of the second Kondo temperature, which is a special feature of the $S = 1$ model and is not found for other integer spins.

We conclude by noting that taking the magnetic anisotropy effects into account is essential in interpreting scanning tunneling spectra of magnetic impurities measured at low temperatures ($T \ll |D|$). The appropriate low-temperature effective impurity model depends on the parameters of the original physical model. While most interpretations of the surface Kondo effect have been based on the Anderson impurity model (which maps on the isotropic Kondo model), it is more likely that the appropriate effective model is, in fact, some anisotropic Kondo model. This is especially true for impurities on decoupling layers, but also applies to impurities adsorbed directly on metallic surface where due to stronger hybridisation charge fluctuation effects also play a role. Appropriate description in terms of an anisotropic model has important consequences on the relation between the Kondo temperature and the “bare” model parameters (effective bandwidth, exchange constants J_\perp and J_z), and on the coupling of the effective impurity spin with the external magnetic field.

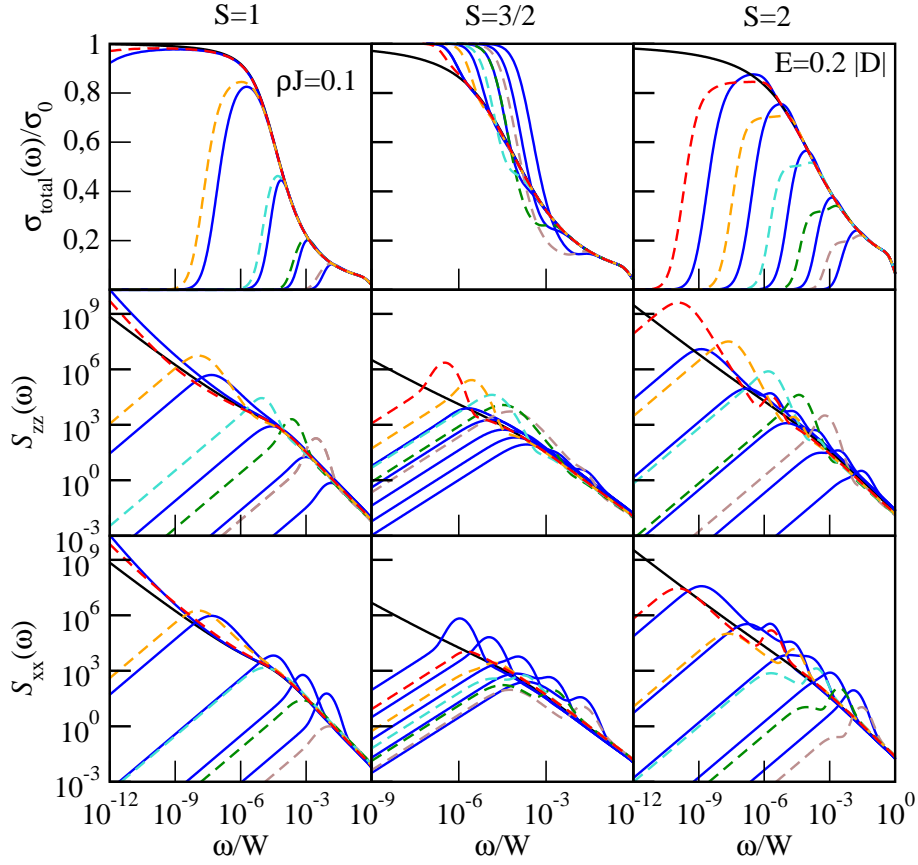


Figure 12: (Color online) Dynamic properties of the anisotropic Kondo model with the $E(S_x^2 - S_y^2)$ term. $E = 0.2|D|$. The curve styles are the same as in Fig. 2.

Appendix A: ANALYSIS OF THE NON-FERMI-LIQUID FIXED POINT

We study the properties of the non-Fermi-liquid fixed point in the $S = 1$ Kondo model with $D < 0$ in the extreme anisotropic limit, $|D| \rightarrow \infty$ (numerical results, where needed, are taken from a $D = -100W$ calculation).

We show that in the $N \rightarrow \infty$ limit (N being the NRG iteration number), the fixed point corresponds to fermions with residual anisotropic exchange scattering from a $S_z = \pm 1$ magnetic doublet. In other words, there is no decoupling of the residual impurity spin, as in the isotropic $S = 1$ Kondo model³⁵. There is furthermore no effective potential scattering in the $|D| \rightarrow \infty$ limit, since the conduction band electrons cannot flip the impurity spin due to the high energy barrier, thus there can be no quasiparticle phase shift due to Kondo screening. We may thus take the Hamiltonian for the uncoupled conduction band chain³⁵

$$H_{\text{band}} = \xi^{-1} \Lambda^{-(N-1)/2} \sum_r \left(E_p^{(0)} p_{r,\sigma}^\dagger p_{r,\sigma} + E_h^{(0)} h_{r,\sigma}^\dagger h_{r,\sigma} \right), \quad (\text{A1})$$

where p and h are second quantization operators for particle and hole excitations, while $E_p^{(0)}$ and $E_h^{(0)}$ are their energies in the units of the characteristic energy scale at the N -th NRG

iteration, and $\xi = \ln \Lambda \sqrt{\Lambda} / (1 - \Lambda^{-1}) \approx 2.41$ is an additional scale factor in the discretization scheme used in this work⁹⁹.

The fixed-point Hamiltonian can be written as $H' = H_{\text{band}} + H_c$ with

$$H_c = J_z^* s_z S_z + J_\perp^* (s_x S_x + s_y S_y), \quad (\text{A2})$$

where s_i are the spin operators on the first site of the Wilson chain,

$$s_i = \sum_{\alpha\alpha'} f_{0,\alpha}^\dagger \left(\frac{1}{2} \sigma_{\alpha\alpha'}^i \right) f_{0,\alpha'}, \quad (\text{A3})$$

while S_i are the impurity spin-1 operators. The f_0 operators need to be written in terms of the single particle and hole operators⁷⁴:

$$f_{0\sigma}^\dagger = \sum_r \alpha_{0r} (p_{r,\sigma}^\dagger + h_{r,\sigma}). \quad (\text{A4})$$

In the $|D| \rightarrow \infty$ limit, the Hilbert space is restricted to the $S_z = \pm 1$ states, thus the transverse exchange J_\perp^* drops out. Keeping only the terms involving the particle excitations, we finally obtain

$$H_c = J_z^* \sum_{r,r'} \alpha_{0r} \alpha_{0r'} S_z \frac{1}{2} \left(p_{r,\uparrow}^\dagger p_{r',\uparrow} - p_{r,\downarrow}^\dagger p_{r',\downarrow} \right). \quad (\text{A5})$$

Energy	Q	S_z	Degeneracy
0	0	± 1	2
0.672864	± 1	$\pm 1/2$	4
0.820964	± 1	$\pm 3/2$	4
1.345728	0	0	2
1.493829	$\pm 2, 0[\times 2]$	± 1	8
1.641929	0	± 2	2

Table I: Excitation spectrum for large negative D (here $D = -100W$, $\Lambda = 2.5$, $N = 79$). The lowest single-particle excitations for free electrons is $E_{p,1}^{(0)} = 0.7468559$.

The fixed-point excitation spectrum computed using NRG is shown in Table I. The ground state has total charge $Q = 0$ and consists of two spin states $S_z = \pm 1$. There are four low-lying single-particle excited states with $Q = +1$: two degenerate levels with $S_z = \pm 1/2$ and (scaled) energy

$$E_p(A) = E_{p,1}^{(0)} - \frac{1}{2} J_z^* \alpha_{01}^2 \Lambda^{(N-1)/2} \xi \quad (\text{A6})$$

and two other degenerate levels with $S_z = \pm 3/2$ and energy

$$E_p(B) = E_{p,1}^{(0)} + \frac{1}{2} J_z^* \alpha_{01}^2 \Lambda^{(N-1)/2} \xi \quad (\text{A7})$$

In the first two levels, the impurity spin and the spin of the particle excitation are anti-aligned, while in the second two levels the impurity spin and the spin of the particle are aligned.

Since the energy difference between $E_p(A)$ and $E_p(B)$ no longer varies with N at the fixed point and the factor $\overline{\alpha}_{01}^2 = \alpha_{01}^2 \Lambda^{(N-1)/2}$ reaches its limiting value (equal to 0.309 for $\Lambda = 2.5$) this implies that J_z^* is a constant given by

$$J_z^* = \frac{E_p(B) - E_p(A)}{\overline{\alpha}_{01}^2 \xi}. \quad (\text{A8})$$

For $\rho J = 0.1$ and $D = -100W$ (Table I) we obtain

$$J_z^* \approx 0.198W = 0.99J. \quad (\text{A9})$$

As expected, we obtain J_z^* which is essentially equal to the bare J in the large- $|D|$ limit.

ACKNOWLEDGMENTS

We thank A. Heinrich for sharing unpublished results for tunneling spectra of Co impurities. We acknowledge support by Gesellschaft für wissenschaftliche Datenverarbeitung (GWDG) in Göttingen through SFB 602 (T. P. and R. Ž.) and project PR 298/10-1 (R.P.).

- ¹ S. Heinze, M. Bode, O. Pietzsch, A. Kubetzka, X. Nie, S. Blügel, and R. Wiesendanger, *Science* **288**, 1805 (2000).
- ² C. A. F. Vaz, J. A. C. Bland, and G. Lauhoff, *Rep. prog. phys.* **71**, 056501 (2008).
- ³ R. Wiesendanger, I. V. Shvets, Dürigler, G. Tarrach, H. J. Güntherodt, J. M. D. Cody, and S. Gräser, *Science* **255**, 583 (1992).
- ⁴ M. Farle, *Rep. Prog. Phys.* **61**, 755 (1998).
- ⁵ P. Gambardella, A. Dallmeyer, K. Maiti, M. C. Malagoli, W. Eberhardt, K. Kern, and C. Carbone, *Nature* **416**, 301 (2002).
- ⁶ S. Rusponi, T. Cren, N. Weiss, P. Bulushek, L. Claude, and H. Brune, *Nature Materials* **2**, 546 (2003).
- ⁷ W. Kuch, *Nature materials* **2**, 505 (2003).
- ⁸ A. J. Heinrich, J. A. Gupta, C. P. Lutz, and D. M. Eigler, *Science* **306**, 466 (2004).
- ⁹ M. Bode, M. Heide, K. von Bergmann, P. Ferriani, S. Heinze, G. Bihlmayer, A. Kubetzka, O. Pietzsch, S. Blügel, and R. Wiesendanger, *Nature* **447**, 190 (2007).
- ¹⁰ C. F. Hirjibehedin, C.-Y. Lin, A. F. Otte, M. Ternes, C. P. Lutz, B. A. Jones, and A. J. Heinrich, *Science* **317**, 1199 (2007).
- ¹¹ P. Ferriani, K. von Bergmann, E. Y. Vedmedenko, S. Heinze, M. Bode, M. Heide, G. Bihlmayer, S. Blügel, and R. Wiesendanger, *Phys. Rev. Lett.* **101**, 027201 (2008).
- ¹² P. Gambardella, S. Rusponi, M. Veronese, S. S. Dhese, C. Grazioli, A. Dallmeyer, I. Cabria, R. Zeller, P. H. Dederichs, K. Kern, et al., *Science* **300**, 1130 (2003).
- ¹³ A. C. Hewson, *The Kondo Problem to Heavy-Fermions* (Cambridge University Press, Cambridge, 1993).
- ¹⁴ R. Bulla, T. Costi, and T. Pruschke, *Rev. Mod. Phys.* **80**, 395 (2008).
- ¹⁵ O. Újsághy, A. Zawadowski, and B. L. Gyorffy, *Phys. Rev. Lett.* **76**, 2378 (1996).
- ¹⁶ O. Újsághy and A. Zawadowski, *Phys. Rev. B* **60**, 10602 (1999).
- ¹⁷ L. Szunyogh, G. Zaránd, S. Gallego, M. C. Muñoz, and B. L. Gyorffy, *Phys. Rev. Lett.* **96**, 067204 (2006).
- ¹⁸ A. Szilva, S. Gallego, M. C. Muñoz, B. L. Gyorffy, G. Zaránd, and L. Szunyogh, *Friedel oscillations induced surface magnetic anisotropy*, arxiv:0805.3275 (2008).
- ¹⁹ C. Etz, J. Zabloudil, P. Weinberger, and E. Y. Vedmedenko, *Phys. Rev. B* **77**, 184425 (2008).
- ²⁰ V. Madhavan, W. Chen, T. Jamneala, M. Crommie, and N. S. Wingreen, *Science* **280**, 567 (1998).
- ²¹ J. Li, W.-D. Schneider, R. Berndt, and B. Delley, *Phys. Rev. Lett.* **80**, 2893 (1998).
- ²² O. Ujsaghy, J. Kroha, L. Szunyogh, and A. Zawadowski, *Phys. Rev. Lett.* **85**, 2557 (2000).
- ²³ A. Schiller and S. Hershfield, *Phys. Rev. B* **61**, 9036 (2000).
- ²⁴ V. Madhavan, W. Chen, T. Jamneala, M. F. Crommie, and N. S. Wingreen, *Phys. Rev. B* **64**, 165412 (2001).
- ²⁵ A. J. Heinrich, private communication.
- ²⁶ H. B. Heersche, Z. de Groot, J. A. Folk, H. S. J. van der Zant, C. Romeike, M. R. Wegewijs, L. Zoppi, D. Barreca, E. Tondello, and A. Cornia, *Phys. Rev. Lett.* **96**, 206801 (2006).
- ²⁷ M. Jo, J. Grose, K. Baheti, M. Deshmukh, J. Sokol, E. Rumberger, D. Hendrickson, J. Long, H. Park, and D. Ralph, *Nano Lett.* **6**, 2014 (2006).
- ²⁸ C. Romeike, M. R. Wegewijs, W. Hofstetter, and H. Schoeller, *Phys. Rev. Lett.* **96**, 196601 (2006).
- ²⁹ C. Romeike, M. R. Wegewijs, W. Hofstetter, and H. Schoeller, *Phys. Rev. Lett.* **97**, 206601 (2006).

- ³⁰ D. Roosen, M. R. Wegewijs, and W. Hofstetter, Phys. Rev. Lett. **100**, 087201 (2008).
- ³¹ L. Bogani and W. Wernsdorfer, Nature materials **7**, 179 (2008).
- ³² D. M. Cragg and P. Lloyd, J. Phys. C: Solid State Phys. **12**, L215 (1979).
- ³³ D. M. Cragg, P. Lloyd, and P. Nozières, J. Phys. C: Solid St. Phys. **13**, 803 (1980).
- ³⁴ P. Mehta, N. Andrei, P. Coleman, L. Borda, and G. Zaránd, Phys. Rev. B **72**, 014430 (2005).
- ³⁵ W. Koller, A. C. Hewson, and D. Meyer, Phys. Rev. B **72**, 045117 (2005).
- ³⁶ K. Furuya and J. H. Lowenstein, Phys. Rev. B **25**, 5935 (1982).
- ³⁷ N. Andrei, K. Furuya, and J. H. Lowenstein, Rev. Mod. Phys. **55**, 331 (1983).
- ³⁸ N. Andrei and C. Destri, Phys. Rev. Lett. **52**, 364 (1984).
- ³⁹ N. Andrei, *Integrable models in condensed matter physics*, condmat/9408011 (1994).
- ⁴⁰ P. D. Sacramento and P. Schlottmann, Phys. Rev. B **40**, 431 (1989).
- ⁴¹ P. D. Sacramento and P. Schlottmann, J. Phys.: Condens. Matter **3**, 9687 (1991).
- ⁴² P. Nozières and A. Blandin, J. Physique **41**, 193 (1980).
- ⁴³ P. Coleman and C. Pepin, Phys. Rev. B **68**, 220405(R) (2003).
- ⁴⁴ M. Bortz and A. Klümper, Eur. Phys. J. B **40**, 25 (2004).
- ⁴⁵ D. C. Mattis, Phys. Rev. Lett. **19**, 1478 (1967).
- ⁴⁶ P. Schlottmann, Phys. Rev. Lett. **84**, 1559 (2000).
- ⁴⁷ P. Schlottmann, J. Appl. Phys. **89**, 7183 (2001).
- ⁴⁸ A. Posazhennikova and P. Coleman, Phys. Rev. Lett. **94**, 036802 (2005).
- ⁴⁹ A. Posazhennikova, B. Bayani, and P. Coleman, Phys. Rev. B **75**, 245329 (2007).
- ⁵⁰ M. Vojta, R. Bulla, and W. Hofstetter, Phys. Rev. B **65**, 140405(R) (2002).
- ⁵¹ P. S. Cornaglia and D. R. Grempel, Phys. Rev. B **71**, 075305 (2005).
- ⁵² R. Žitko and J. Bonča, Phys. Rev. B **73**, 035332 (2006).
- ⁵³ C.-H. Chung, G. Zaránd, and P. Wölfle, Phys. Rev. B **77**, 035120 (2008).
- ⁵⁴ R. Žitko and J. Bonča, Phys. Rev. B **74**, 045312 (2006).
- ⁵⁵ R. Žitko and J. Bonča, Phys. Rev. B **76**, 241305(R) (2007).
- ⁵⁶ W. Izumida, O. Sakai, and S. Tarucha, Phys. Rev. Lett. **87**, 216803 (2001).
- ⁵⁷ M. Pustilnik and L. I. Glazman, Phys. Rev. Lett. **87**, 216601 (2001).
- ⁵⁸ M. Pustilnik and L. I. Glazman, Phys. Rev. B **64**, 045328 (2001).
- ⁵⁹ O. Sakai and W. Izumida, Physica B **328**, 125 (2003).
- ⁶⁰ M. Pustilnik, L. I. Glazman, and W. Hofstetter, Phys. Rev. B **68**, 161303(R) (2003).
- ⁶¹ W. Hofstetter and G. Zaránd, Phys. Rev. B **69**, 235301 (2004).
- ⁶² J. Schmid, J. Weis, K. Eberl, and K. v. Klitzing, Phys. Rev. Lett. **84**, 5824 (2000).
- ⁶³ S. Sasaki, S. de Franceschi, J. M. Elzerman, W. G. van der Wiel, M. Eto, S. Tarucha, and L. P. Kouwenhoven, Nature **405**, 764 (2000).
- ⁶⁴ W. G. van der Wiel, S. De Franceschi, J. M. Elzerman, S. Tarucha, L. P. Kouwenhoven, J. Motohisa, F. Nakajima, and T. Fukui, Phys. Rev. Lett. **88**, 126803 (2002).
- ⁶⁵ A. Kogan, G. Granger, M. A. Kastner, D. Goldhaber-Gordon, and H. Shtrikman, Phys. Rev. B **67**, 113309 (2003).
- ⁶⁶ A. Fuhrer, T. Ihn, K. Ensslin, W. Wegscheider, and M. Bichler, Phys. Rev. Lett. **91**, 206802 (2003).
- ⁶⁷ G. Granger, M. A. Kastner, I. Radu, M. P. Hanson, and A. C. Gossard, Phys. Rev. B **72**, 165309 (2005).
- ⁶⁸ R. M. Konik, H. Saleur, and A. W. W. Ludwig, Phys. Rev. B **66**, 075105 (2002).
- ⁶⁹ A. Schiller and L. De Leo, Phys. Rev. B **77**, 075114 (2008).
- ⁷⁰ P. W. Anderson, J. Phys. C: Solid St. Phys. **3**, 2436 (1970).
- ⁷¹ A. M. Tsvelick and P. B. Wiegmann, Adv. Phys. **32**, 453 (1983).
- ⁷² T. A. Costi and C. Kieffer, Phys. Rev. Lett. **76**, 1683 (1996).
- ⁷³ T. A. Costi, Phys. Rev. Lett. **80**, 1038 (1998).
- ⁷⁴ K. G. Wilson, Rev. Mod. Phys. **47**, 773 (1975).
- ⁷⁵ H. R. Krishna-murthy, J. W. Wilkins, and K. G. Wilson, Phys. Rev. B **21**, 1003 (1980).
- ⁷⁶ D. Kaihe and B.-H. Zhao, Phys. Lett. A **340**, 337 (2005).
- ⁷⁷ N. Andrei and J. H. Lowenstein, Phys. Rev. Lett. **46**, 356 (1981).
- ⁷⁸ C. Jayaprakash, H. R. Krishna-murthy, and J. W. Wilkins, Phys. Rev. Lett. **47**, 737 (1981).
- ⁷⁹ R. Peters and T. Pruschke, New Journal of Physics **8**, 127 (2006).
- ⁸⁰ C. Gonzalez-Buxton and K. Ingersent, Phys. Rev. B **57**, 14254 (1998).
- ⁸¹ S. Florens and M. Vojta, Phys. Rev. B **72**, 115117 (2005).
- ⁸² D. Withoff and E. Fradkin, Phys. Rev. Lett. **64**, 1835 (1990).
- ⁸³ K. Chen and C. Jayaprakash, J. Phys.: Condens. Matter **7**, L491 (1995).
- ⁸⁴ M. Vojta and R. Bulla, Eur. Phys. J. B **28**, 283 (2002).
- ⁸⁵ T. A. Costi, A. C. Hewson, and V. Zlatic, J. Phys.: Condens. Matter **6**, 2519 (1994).
- ⁸⁶ W. Hofstetter, Phys. Rev. Lett. **85**, 1508 (2000).
- ⁸⁷ R. Peters, T. Pruschke, and F. B. Anders, Phys. Rev. B **74**, 245114 (2006).
- ⁸⁸ A. Weichselbaum and J. von Delft, Phys. Rev. Lett. **99**, 076402 (2007).
- ⁸⁹ T. A. Costi, Phys. Rev. Lett. **85**, 1504 (2000).
- ⁹⁰ G. Zaránd, L. Borda, J. von Delft, and N. Andrei, Phys. Rev. Lett. **93**, 107204 (2004).
- ⁹¹ L. Borda, L. Fritz, N. Andrei, and G. Zaránd, Phys. Rev. B **75**, 235112 (2007).
- ⁹² M. Vojta, R. Zitzler, R. Bulla, and T. Pruschke, Phys. Rev. B **66**, 134527 (2002).
- ⁹³ P. S. Cornaglia and C. A. Balseiro, Phys. Rev. B **67**, 205420 (2003).
- ⁹⁴ A. V. Balatsky, Y. Manassen, and R. Salem, Phys. Rev. B **66**, 195416 (2002).
- ⁹⁵ Z. Nussinov, M. F. Crommie, and A. V. Balatsky, Phys. Rev. B **68**, 085402 (2003).
- ⁹⁶ M. Garst, P. Wölfle, L. Borda, J. von Delft, and L. Glazman, Phys. Rev. B **72**, 205125 (2005).
- ⁹⁷ H. Shiba, Prog. Theor. Phys. **54**, 967 (1975).
- ⁹⁸ W. Hofstetter and S. Kehrein, Phys. Rev. B **63**, 140402(R) (2001).
- ⁹⁹ V. L. Campo and L. N. Oliveira, Phys. Rev. B **72**, 104432 (2005).